ACS OMEGA

Open Access

http://pubs.acs.org/journal/acsodf

Article

Effect of Adsorption and Interactions of New Triazole-Thione-Schiff Bases on the Corrosion Rate of Carbon Steel in 1 M HCl Solution: Theoretical and Experimental Evaluation

Arafat Toghan,* Omar K. Alduaij, Ahmed Fawzy, Ayman M. Mostafa, Ahmed M. Eldesoky, and Ahmed A. Farag*

Cite This: *ACS Omega* 2024, 9, 6761−6772

Read Online

ACCESS | Metrics & More | Article Recommendations

ABSTRACT: Due to the unique properties of steel, including its hardness, durability, and superconductivity, which make it an essential material in many industries, it lacks corrosion resistance. Herewith, two novel triazole-thione Schiff bases, namely, (*E*)-5-methyl-4-((thiophen-2-ylmethylene)amino)-2,4-dihydro-3*H*-1,2,4-triazole-3-thione (TMAT) and (*E*)-4-(((5-(dimethylamino)thiophen-2-yl)methylene)amino)-5-methyl-2,4-dihydro-3*H*-1,2,4-triazole-3-thione (DMTMAT), were synthesized and characterized. The corrosion inhibition (CI) ability of these two molecules on carbon steel in an aqueous solution of 1 M HCl as well as their interaction with its surface was studied using a number of different techniques. The results confirmed that the CI capability of these organic molecules depends on their strong adsorption on the metal surface and the formation of a protective anticorrosion film. Weight loss tests revealed that the inhibition efficiencies of TMAT and DMTMAT were 91.1 and 94.0%, respectively, at 1 × 10^{-3} M concentrations. The results of electrochemical impedance spectroscopy (EIS) indicated that there was a direct relationship between the inhibitor concentration and the transfer resistance. Potentiodynamic polarization (PDP) experiments have proven to be mixed-type inhibitors of C-steel in aqueous hydrochloric acid solution and follow the Langmuir adsorption isotherm model. Several thermodynamic and kinetic parameters were calculated. The negative values of the adsorption-free energy are −36.7 and −38.5 kJ/mol for TMAT and DMTMAT, respectively, confirming the spontaneity of the adsorption process. The MD simulation study's findings show that the inhibitor molecules are nearly parallel to the metal surface. The interaction energy calculated by the MD simulation and the inhibitory trend are the same. The practical implementation is consistent with what the computer models predicted.

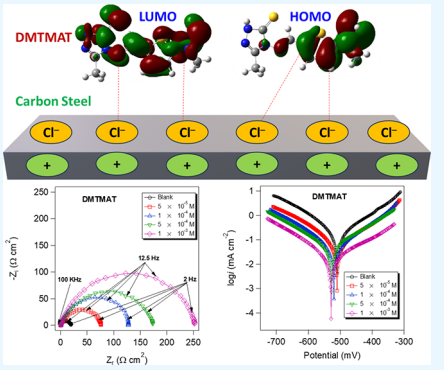

1. INTRODUCTION

Carbon steel is commonly exposed to acids in a variety of operations, including industrial acid cleaning, oil well acidification, acid descaling, and metal acid pickling, especially in 1.0 M HCl solution.[1−4] In such hostile settings, heterocycles are commonly utilized as corrosion inhibitors due to their wide availability and diversity, which considerably slows metal corrosion.[5−15] Metal corrosion resistance varies based on how strongly organic molecules attach to metal surfaces and prevent corrosion.[16−21] Many bonds, aromatic rings, nitrogen, sulfur, and oxygen are typically found in the most effective inhibitors.[22] However, traditional inhibitors have drawbacks such as toxicity. As a result, investigations on green and environmentally acceptable corrosion inhibitors have primarily focused on research on effective but less expensive compounds with less environmental impact.[23] The subject of greater research in this area has been a variety of substances, including plant extracts, Schiff bases, thiosemicarbazones, amino acids, and triazole derivatives. As a result, Schiff bases might be considered a fast-evolving potential unit in the field of heterocyclic chemistry, with very promising qualities and applications in corrosion inhibition.[24,25] All of these qualities are nontoxic.[26] It is also worth noting that the most important thing that distinguishes Schiff bases from other materials is that they are environmentally safe materials and easy to prepare, which makes them used in a wide range of applications, especially medical and pharmaceutical applications, including anti-inflammatory, analgesic, antibacterial, anticancer, and antioxidants, in addition to being effective corrosion inhibitors. Particularly, triazoles and their derivatives are effective corrosion inhibitors. These compounds likely have enhanced adsorption on metal surfaces under abrasive conditions due to

Received: October 16, 2023
Revised: January 9, 2024
Accepted: January 19, 2024
Published: February 2, 2024

their polar groups and their ability to form complexes with the metal surface, which is also one of their advantages. Additionally, the nitrogen atom has a large number of π-electrons and unshared electron pairs, which interact with any metal's d-orbitals to produce a shielding layer.[27] As a result, recent years have seen a lot of interest in the study of 1,2,4-derivative triazole inhibitors. Numerous investigations have been done on novel triazole compounds to improve the efficiency of triazole derivatives as inhibitors.[28] However, researchers are still interested so far in improving the heterocycle's ability to further suppress metallic corrosion. One strategy for this is to add extra moieties or functional groups to their structure.[16,29−32] Based on the above, it is clear that the unique structure of Schiff bases contains electron-donating nitrogen atoms, which makes them act as strong chelating agents that like to chemically attach to the metal surface. Not only this but also in acidic environments, they can be protonated, which helps them physically adsorb to the metal surface to form a protective corrosion layer. Accordingly, two brand-new inexpensive triazole-thione-Schiff bases were developed, namely, (*E*)-5-methyl-4-((thiophen-2-ylmethylene)amino)-2,4-dihydro-3*H*-1,2,4-triazole-3-thione (TMAT), and (*E*)-4-(((5-(dimethylamino)thiophen-2-yl)-methylene)amino)-5-methyl-2,4-dihydro-3*H*-1,2,4-triazole-3-thione (DMTMAT). Their inhibition anticorrosion capability to the carbon steel in 1 M HCl was investigated using different chemical, electrochemical, spectroscopic, and computational methods.

2. EXPERIMENTAL SECTION

2.1. Preparation of Indole-3-aldehydehyde and Dipeptide Schiff Bases. To produce TMAT and DMTMAT, 25 mL of ethanol, 5 mmol of 4-amino-5-methyl-2,4-dihydro-3*H*-1,2,4-triazole-3-thione, and 5 mmol of either thiophene-2-carbaldehyde, or 5-dimethylamino-thiophene-2-carbaldehyde was added to a flask with a round bottom. As a catalyst for the process, a little amount of *p*-toluene sulfonic acid (TSA) was introduced.[33] After that, the reactant solutions were refluxed for another 6 h. After the precipitated material was cooled to room temperature, it was filtered, extensively washed with ethanol, and dried under reduced pressure to yield (*E*)-5-methyl-4-((thiophen-2-ylmethylene)amino)-2,4-dihydro-3*H*-1,2,4-triazole-3-thione (TMAT), and (*E*)-4-(((5-(dimethylamino)thiophen-2-yl)methylene)amino)-5-methyl-2,4-dihydro-3*H*-1,2,4-triazole-3-thione (DMTMAT). Table 1 represents the chemical structures, IUPAC names, and abbreviations of the prepared Schiff bases. ^{1}H NMR of TMAT (400 MHz, $CDCl_3$) δ: 2.3 (3H, terminal C$\underline{H}_3$ attached to triazole ring), 7.3−7.9 (3H, aromatic thiophene ring), 10.0 (H, =N−C$\underline{H}$ of imine bond), and 14.2 (1H for N$\underline{H}$ of triazole group). ^{1}H NMR of DMTMAT (400 MHz, $CDCl_3$) δ: 2.3 (3H, terminal C$\underline{H}_3$ attached to triazole ring), 3.2 (6H, terminal 2C$\underline{H}_3$ attached to nitrogen atom attached to thiophene ring), 6.1, 6.9 (2H, of aromatic thiophene ring), 10.0 (H, =N−C$\underline{H}$ of imine bond), and 14.4 (1H for N$\underline{H}$ of triazole group).

Table 1. Structures, IUPAC Names, and Abbreviations of TMAT and DMTMAT Schiff Bases

Inhibitor structure	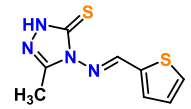	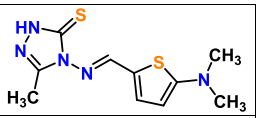
IUPAC name	(E)-5-methyl-4-((thiophen-2-ylmethylene)amino)-2,4-dihydro-3H-1,2,4-triazole-3-thione	(E)-4-(((5-(dimethylamino)thiophen-2-yl)methylene)amino)-5-methyl-2,4-dihydro-3H-1,2,4-triazole-3-thione
Abbreviation	TMAT	DMTMAT

2.2. Steel and Solution Preparation. The elemental composition (wt %) of the carbon steel employed in this work is as follows: C (0.22), Si (0.36), P (0.08), Mn (0.04), Al (0.01), S (0.04), and Fe balance. Analytical-grade 37% HCl was diluted with distilled water to make a 1 M HCl solution. The synthetic TMAT and DMTMAT molecules are dissolved in the acidic solution to be evaluated at dosages ranging from 10^{-5} to 10^{-3} M.

2.3. Weight Loss Method. Before the final cleaning process, the carbon steel was cut into coupons with dimensions of 5 × 2 × 0.2 cm and the carbon steel samples were abraded using various grades of silicon carbide abrasive sheets (400−1200). These abraded samples were cleaned twice with acetone to remove any contaminants and then dried. The materials were carefully weighed and immersed for 8 h in a 1 M HCl solution without and with various dosages of TMAT and DMTMAT inhibitors. Following that, the specimens were carefully removed, washed, dried, and weighed again.[34]

2.4. Electrochemical Measurements. Analytical software (VoltaMaster 4) was used to control an electrochemical potentiostat of the PGZ 400 type. Three electrode systems were used: platinum as an auxiliary electrode, saturated calomel electrode (SCE) as a reference, and carbon steel as a working electrode. The polarization curves were obtained by shifting the electrode potential from −800 to −200 mV at a scanning rate of 0.1 mV/s. The EIS test was carried out at the OCP with a frequency range of 100 kHz to 10 mHz and a peak-to-peak amplitude of 10 mV AC signal.

2.5. DFT and MD Simulation Investigation. The quantum chemical modeling results were obtained using Gaussian software 9.0. The computations were performed using the density functional theory (DFT) baseline set 6-31*G(d,p). The following equations can be written using Koopmans' theorem:[35,36]

$$\Delta E = \mathrm{IP} - \mathrm{EA} = -E_{\mathrm{HOMO}} + E_{\mathrm{LUMO}} \quad (1)$$

$$\Delta N = \frac{(\chi_{\mathrm{Fe}} - \chi_{\mathrm{Inh}})}{2(\eta_{\mathrm{Fe}} + \eta_{\mathrm{Inh}})} \quad (2)$$

$$\chi = \frac{\mathrm{IP} + \mathrm{EA}}{2} \quad (3)$$

$$\eta = \frac{\mathrm{IP} - \mathrm{EA}}{2} \quad (4)$$

where IP denotes the ionization potential and EA denotes the electron affinity. ΔE is the energy difference between the energy of the least unoccupied molecular orbital (E_{LUMO}) and the energy of the highest occupied molecular orbital (E_{HOMO}). Hardness and chemical electronegativity are indicated by η and χ, respectively. ΔN denotes the electrons that transfer from the inhibitor to a metal surface. The intensity of the interactions between the examined chemical and iron surface was determined using molecular dynamics (MD) simulations. These simulations were carried out by using the Materials Studio software. The Fe (110) surface was employed with the COMPASS force field, 303 K temperature, NVT ensemble,

https://doi.org/10.1021/acsomega.3c08127
ACS Omega 2024, 9, 6761−6772

and a time step of 1 fs were the details used in these simulations.

3. RESULTS AND DISCUSSION

3.1. Weight Loss Studies. Table 2 displays the TMAT and DMTMAT concertation variation concerning the

Table 2. Weight Loss Parameters for the Carbon Steel Corrosion in 1 M HCl without and with Different Concentrations of Inhibitors at Temperature of 298 K

inhibitor	conc. (M)	ν (mg h^{-1} cm^{-2})	θ	η_{WL} (%)
blank	0	7.115 ± 0.321		
TMAT	5×10^{-5}	1.978 ± 0.102	0.722	72.2
	1×10^{-4}	1.153 ± 0.060	0.838	83.8
	5×10^{-4}	0.989 ± 0.045	0.861	86.1
	1×10^{-3}	0.633 ± 0.023	0.911	91.1
DMTMAT	5×10^{-5}	1.764 ± 0.082	0.752	75.2
	1×10^{-4}	0.875 ± 0.029	0.877	87.7
	5×10^{-4}	0.690 ± 0.017	0.903	90.3
	1×10^{-3}	0.427 ± 0.0113	0.940	94.0

corrosion rate, ν (mg h^{-1} cm^{-2}), and the inhibition efficiency (η%). Using the following formulas, the corrosion rate (ν), surface coverage (θ), and inhibition effectiveness are determined:[37]

$$\nu = \frac{\Delta W}{St} \tag{5}$$

$$\theta = \frac{CR - CR_{inh}}{CR} \tag{6}$$

$$\eta(\%) = \theta \times 100 \tag{7}$$

where CR and CR_{inh} represent, respectively, the rates of steel corrosion in 1 M HCl in the absence and presence of various concentrations of TMAT and DMTMAT. ΔW, S, and t stand for weight loss (in grams), carbon steel surface area (in square meters), and length of immersion (in hours).

The variation of TMAT and DMTMAT concentrations with the obtained corrosion rates and inhibition efficiencies at a temperature of 298 K are plotted in Figure 1. One can infer from Figure 1 data that an increase in TMAT and DMTMAT concentration causes an increase in % and a decrease in ν values. The amount of TMAT and DMTMAT inhibitors covering the coupon increases as the inhibitor concentration rises, reflecting an increase in the number of adsorbed inhibitors (θ) as a result of the concentration increase.[38] This concentration is thought to act as an isolation barrier between the carbon steel and the aggressive HCl solution interface, preventing the action of corrosive ions on the steel. Table 2 makes it quite evident that the DMTMAT inhibitor is more effective than the TMAT inhibitor. This is because the dimethyl amino chain of the DMTMAT inhibitor is growing, increasing its adsorption strength at the carbon steel surface and delaying the aggressive solution, which enhances the effectiveness of corrosion inhibition.[39]

3.2. Adsorption Isotherm Investigation. An adsorption isotherm can be used to explain the interactions between carbon steel and Schiff bases (TMAT and DMTMAT). Figure 2 depicts the application of various adsorption isotherm models such as Langmuir, Temkin, Freundlich, and Flory–Huggins to elucidate the kind and strength of adsorption interactions between carbon steel and Schiff bases (TMAT and DMTMAT) at a temperature of 298 K.[40]

The best experimental results were obtained by using the Langmuir adsorption isotherm. Figure 2a shows a linear graph of C/θ vs C, and the estimated correlation coefficient (R^2) is close to unity. This explains why TMAT and DMTMAT adsorptions on the carbon steel surface follow the Langmuir isotherm model. The Langmuir adsorption isotherm was written as[41]

$$\frac{C}{\theta} = \frac{1}{K_{ads}} + C \tag{8}$$

where K_{ads} stands for the adsorption equilibrium constant and C is the inhibitor concentration. The high K_{ads} values in Table 3 show that Schiff base inhibitors have a high capacity for adsorption on the surface of carbon steel. Using the relationship shown below, the standard free energy of adsorption (ΔG^{o}_{ads}) was calculated:[42]

$$K_{ads} = \frac{1}{55.5}\exp\left(\frac{-\Delta G^{o}_{ads}}{RT}\right) \tag{9}$$

where 55.5 represents the concentration of water in the solution (in mol/L), R represents the universal gas constant (8.314 J/mol K), and T represents the absolute temperature (in Kelvin).

Values of ΔG^{o}_{ads} of −20 kJ/mol or less negative are frequently compatible with electrostatic interaction (physisorption), whereas values of −40 kJ/mol or more negative are

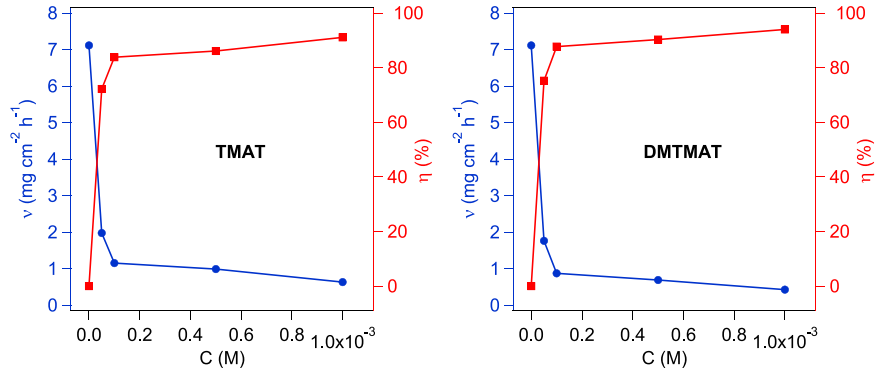

Figure 1. Variation of TMAT and DMTMAT concentrations with corrosion rates and inhibition efficiencies for carbon steel in 1 M HCl solution at temperature of 298 K.

https://doi.org/10.1021/acsomega.3c08127
ACS Omega 2024, 9, 6761−6772

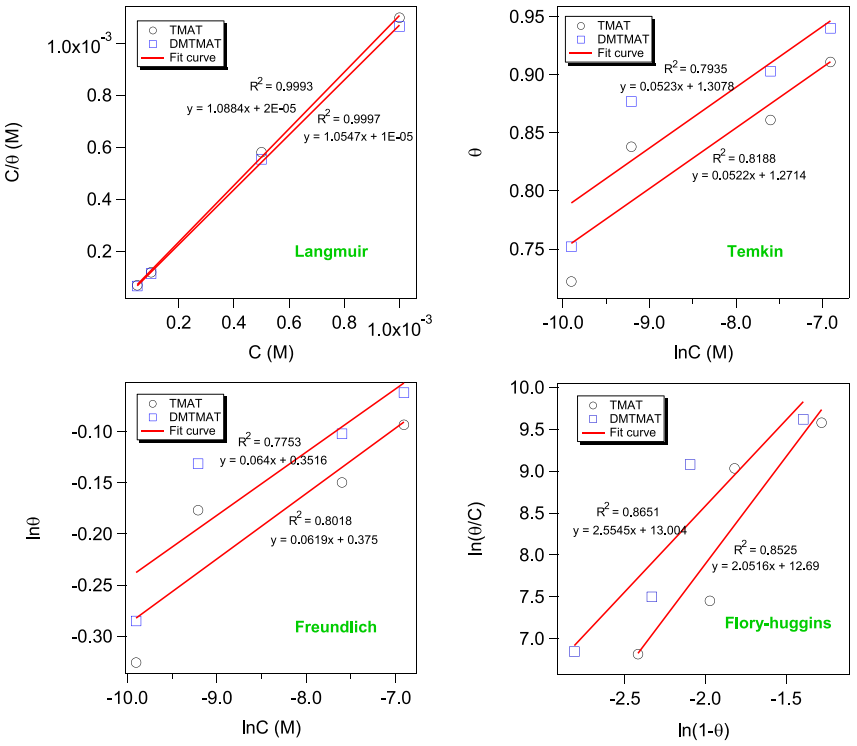

Figure 2. Langmuir, Temkin, Freundlich, and Flory–Huggins adsorption isotherms for TMAT and DMTMAT inhibitors at carbon steel in 1 M HCl solution at temperature of 298 K.

Table 3. Langmuir Thermodynamic Parameters of Carbon Steel in 1 M HCl Solution Containing Inhibitors at Temperature of 298 K

inhibitor	R^2	K_{ads} L/mol	ΔG^{o}_{ads} kJ/mol
TMAT	0.9993	5×10^4	−36.7
DMTMAT	0.9987	10×10^4	−38.5

usually consistent with charge sharing interaction (chemisorption).[43] TMAT and DMTMAT inhibitors (−36.7 and −38.5) may both be adsorbed on the surface of carbon steel to prevent corrosion by physisorption and chemisorption,[44] as demonstrated by the reported ΔG^{o}_{ads} values in Table 3.

3.3. Potentiodynamic Polarization (PDP) Studies. Figure 3 shows the polarization curves of carbon steel both with and without TMAT and DMTMAT inhibitors at a temperature of 298 K. These measures of polarization provide information on cathodic and anodic reactions. Table 4 displays the corrosion potential (E_{corr}), the corrosion current density (i_{corr}), the anodic and cathodic Tafel slopes (β_a, β_c), and the inhibition efficacy (η%). The equation below is used to compute the inhibition efficiency for different inhibitor dosages.[45]

$$\eta\% = \frac{i^{o}_{corr} - i_{corr}}{i^{o}_{corr}} \times 100 \tag{10}$$

where i_{corr} and i^{o}_{corr} stand for the current density with and without the corrosion inhibitors under investigation, respectively.

The polarization curves in 1 M HCl solutions with various dosages of TMAT and DMTMAT inhibitors are strikingly equivalent, as shown in Figure 3. It makes sense that these inhibitors would also restrict the hydrogen evolution reaction, given that both the cathodic and anodic sides of carbon steel electrode corrosion were slowed. Indicating that the hydrogen

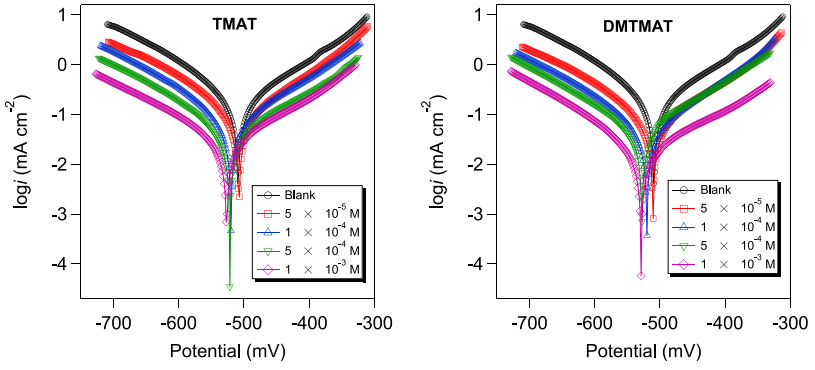

Figure 3. Potentiodynamic polarization plots for carbon steel in 1 M HCl without and with TMAT and DMTMAT inhibitors at a temperature of 298 K.

https://doi.org/10.1021/acsomega.3c08127
ACS Omega 2024, 9, 6761−6772

Table 4. Tafel Factors for the Carbon Steel Corrosion in 1 M HCl without and with Different Concentrations of Inhibitors at Temperature of 298 K

inhibitor	conc. (M)	$-E_{corr}$ (mV vs SCE)	i_{corr} (μA cm^{-2})	β_a (mV day^{-1})	$-\beta_c$ (mV day^{-1})	η_{PDP} (%)
1 M HCl	Blank	509	211.3 ± 6.021	138	173	
TMAT	5×10^{-5}	507	62.0 ± 2.11	144	178	70.7
	1×10^{-4}	520	37.2 ± 1.07	126	149	82.4
	5×10^{-4}	522	27.6 ± 1.12	138	202	87.0
	1×10^{-3}	527	20.6 ± 0.72	145	167	90.3
DMTMAT	5×10^{-5}	511	53.1 ± 2.34	130	156	74.9
	1×10^{-4}	519	30.8 ± 0.89	134	166	85.4
	5×10^{-4}	526	23.1 ± 1.41	140	205	89.1
	1×10^{-3}	528	15.8 ± 0.62	131	153	92.5

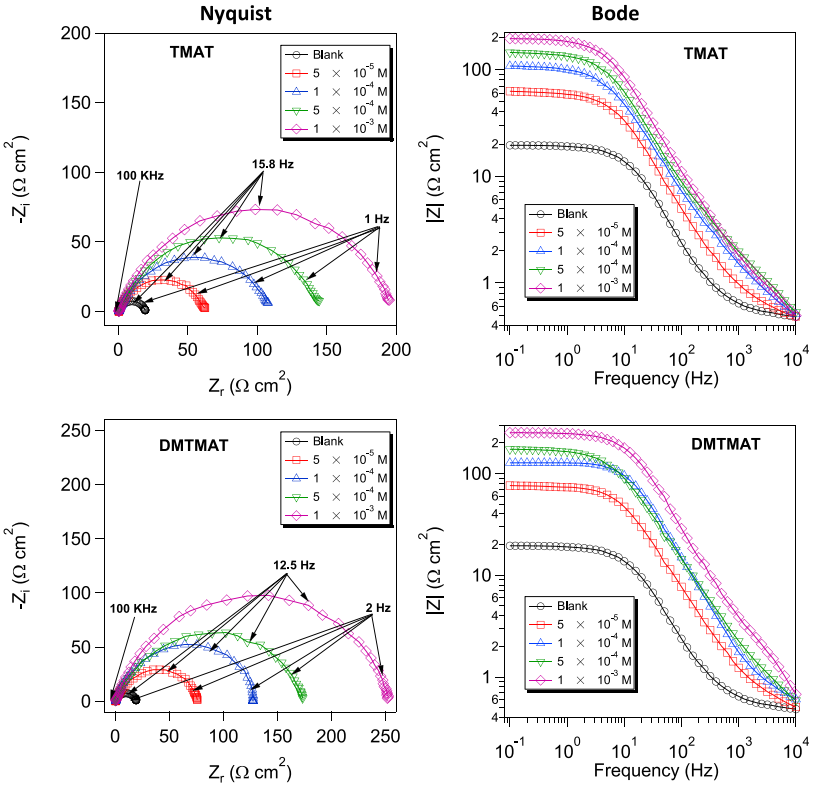

Figure 4. Nyquist and Bode plots for carbon steel in 1 M HCl without and with TMAT and DMTMAT inhibitors at a temperature of 298 K.

evolution reaction is activation regulated and that the addition of the inhibitors does not affect the reduction mechanism other than to block the metal surface, cathodic Tafel curves lead to parallel Tafel lines.[46] The corrosion current density values in the inhibitor-containing solutions were lower than in the control acid solution, as shown in Table 4.

For the inhibitors under study, the corrosion current density decreases and the inhibition efficiency increases with increasing inhibitor concentrations.[47] TMAT and DMTMAT inhibitors have the maximum levels of efficacy, 90.3 and 92.5%, respectively, at a concentration of 10^{-3} M. The DMTMAT inhibitor outperformed TMAT due to the extra dimethyl amino group. This is due to the two methyl groups supporting the nitrogen lone pair electrons, which release electrons to increase the electrical density at the DMTMAT structure.[48] Strikingly, there is a slight difference in the corrosion potential values with changing concentration of both inhibitors, indicating that they behave as mixed-type inhibitors (see Table 4).[49,50] Tafel polarization curve inhibition efficiencies are often lower than those measured by weight loss measures due to the varied experimental settings.

3.4. Electrochemical Impedance Spectroscopy (EIS) Studies. To evaluate changes at the metal/HCl interface in the absence and presence of inhibitor concentration over a given frequency range, EIS is used.[51] Figure 4 displays the Nyquist plots of the outcomes of the EIS tests at a temperature of 298 K that were looked at to do this.

Nyquist diagrams can be used to determine that these curves are composed of a single capacitive semicircle.[52] The deformation of the half-circles is caused by the variability of the working electrodes. The fact that every curve has the same shape, however, demonstrates that the dissolving process still happens regardless of whether an electrolyte is impeded.[53] This suggests that the mechanism behind the corrosion process is made up of just one phase, or an electron charge transfer process and that the amount of inhibitor present has no influence on this mechanism.[54] Contrarily, the inclusion of TMAT and DMTMAT inhibitors can significantly affect the semicircular curve diameters depending on the concentration,

https://doi.org/10.1021/acsomega.3c08127
ACS Omega 2024, 9, 6761−6772

which further demonstrates that their addition has slowed the rate of steel dissolving. The efficiency of the examined inhibitor at inhibiting is calculated using the formula below:[55]

$$\eta\% = \frac{R_{ct}^{i} - R_{ct}^{o}}{R_{ct}^{i}} \times 100 \quad (11)$$

where R_{ct}^{i} and R_{ct}^{o} are the charge transfer resistances in inhibited and inhibitor free solutions. The equivalent circuit model used to match the electrochemical impedance data is depicted in Figure 5, which comprises the solution resistance R_s, polarization resistance R_{ct}, and double-layer capacitance C_{dl}.

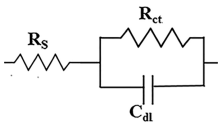

Figure 5. Equivalent circuit model used to fit electrochemical impedance data.

The equation was used to compute the double layer capacitance C_{dl}:[56]

$$C_{dl} = Q(\omega_{max})^{n-1} \quad (12)$$

Where ω_{max} denotes the highest angular frequency.

Table 5 demonstrates that for various TMAT and DMTMAT inhibitor concentrations, R_{ct} and C_{dl} move in opposite directions, i.e., an increase in R_{ct} and a decrease in C_{dl} with an increasing trend in inhibitor quantity. Because the inhibitor's surface covering increased, the inhibition efficiency improved.[57] C_{dl} values drop due to either a decrease in the local dielectric constant or an increase in the thickness of the electric double layer, showing that the inhibitor molecules function by adsorption at the metal/solution interface.[58] The constant displacement of water molecules caused by organic molecule adsorption on the metal surface may also help to reduce the extent of metal dissolution.[59] The Bode-phase diagram (Figure 4) illustrates the evolution of the Z-module as a function of frequency in the acidic 1 M HCl environment without and with different concentrations of the TMAT and DMTMAT inhibitors. This diagram shows the behavior of the inhibitory layer that TMAT and DMTMAT molecules form at the surface of carbon steel as a result of an adsorption process, where the Z-module values increased by increasing the inhibitor concentrations. Finally, the inhibitory efficiencies obtained by electrochemical impedance spectroscopy, polarization, and weight loss tests seem to be completely consistent.

3.5. Molecular Modeling Computations. To identify the variables governing the efficacy of an inhibitor, quantum chemical calculations were used to count the number of molecular and electronic properties.[60] Frontier molecular orbitals of the inhibitor chemicals can be used to predict their interactions with metallic facet. Figure 6 shows the ideal molecular structures and electrostatic potential surfaces (EPS) of TMAT and DMTMAT molecules as well as the HOMO and LUMO molecular density distributions. The designated quantum chemical descriptors are listed in Table 6.

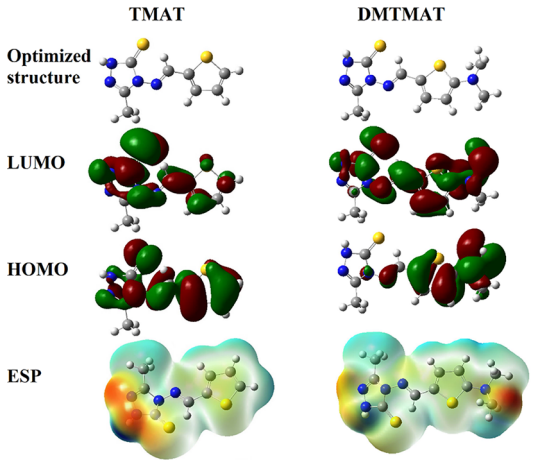

Figure 6. Optimized structure, HOMO, LUMO, and ESP for TMAT and DMTMAT inhibitors.

Table 6. Calculated Quantum Chemical Parameters for TMAT and DMTMAT Inhibitors

parameters	TMAT	DMTMAT
E_{HOMO}	−8.8030	−7.8260
E_{LUMO}	2.0370	2.1610
ΔE	10.8400	9.9870
ΔN	0.3337	0.4173
μ (Debye)	3.6148	2.8930

Understanding the frontier orbitals theory and orbitals like HOMO and LUMO provides a simple method for measuring a species' propensity to supply or receive electrons.[61] However, it is well-known that a molecule's energy gap (ΔE) influences both its stability and, consequently, its reactivity. An efficient corrosion inhibitor should have one because a small ΔE value denotes a high level of reactivity in the molecule.[62] First, the

Table 5. EIS Factors for the Carbon Steel Corrosion in 1 M HCl without and with Different Concentrations of Inhibitors at Tmperature of 298 K

inhibitor	conc (M)	R_s (Ω)	C_{dl} (μF/cm^2)	R_{ct} (Ω cm^2)	X^2	η_{EIS} (%)
1 M HCl	blank	1.8	115.4	19 ± 0.65	0.14	—
TMAT	5×10^{-5}	1.9	32.2	68 ± 1.52	0.58	72.1
	1×10^{-4}	1.9	19.1	115 ± 3.04	0.77	83.5
	5×10^{-4}	2.1	15.1	145 ± 3.54	1.07	86.9
	1×10^{-3}	2.2	11.0	199 ± 6.57	1.19	90.5
DMTMAT	5×10^{-5}	2.5	28.5	77 ± 1.98	0.62	75.3
	1×10^{-4}	2.3	17.1	128 ± 4.05	0.84	85.2
	5×10^{-4}	2.6	12.6	174 ± 5.02	1.21	89.1
	1×10^{-3}	2.4	8.7	253 ± 7.52	1.69	92.5

https://doi.org/10.1021/acsomega.3c08127
ACS Omega 2024, 9, 6761−6772

HOMO and LUMO orbitals, which serve as a graphic representation of the molecule's boundary molecular orbitals, can be used to estimate the inhibitors' efficacy. Based on whether or not they contain a different functional group, Schiff basses differ from one another despite having identical structural makeup.[63] The isodensity in the HOMO and LUMO orbitals of both molecules is dispersed throughout the whole moiety, as seen in Figure 6. Since these moieties are well known for their primary inhibitive activity, we can infer that all compounds should have strong electron-accepting and electron-donating characteristics. The provision of electrons by sulfur and nitrogen frequently has a substantial effect on inhibitor reactivity. However, the border orbital distribution does not adequately capture this influence. To more accurately forecast each compound's reactivity and the impact of its functional groups, quantum chemical characteristics could be used. Low LUMO energy indicates a greater capacity to accept electrons, but high HOMO energy indicates a stronger tendency to donate them.[64] The energy gap (ΔE) is a fundamental concept in quantum chemistry. The molecule's ability for adsorption and, by extension, reactivity, increases with decreasing value.[65] Visual examination of Table 6 made it obvious that the ΔE values matched the DMTMAT < TMAT sequence. The fact that ΔN, the number of electrons supplied by the inhibitor to the metal surface, is positive provides more proof that TMAT and DMTMAT inhibitors are electron givers. Additionally, ΔN suggested that order favors DMTMAT, which goes against the conclusions of the research. The fact that ΔN is less than 3.6 implies an improvement in the ability to donate electrons, which may boost the ability of the TMAT and DMTMAT molecules to inhibit the corrosion of carbon steel surface.[66] Finally, the quantum global descriptors demonstrate that the investigated inhibitor's structure has a high reactivity performance, mirroring the resistance values determined through experiments and therefore explaining their adsorption onto the steel surface, establishing a protective layer. Furthermore, the dipole moment (μ) is a property that may have an impact on the corrosion inhibition of the carbon steel.[67] The tested chemical in this study has values of 3.6D and 2.9D for TMAT and DMTMAT molecules, respectively, which is substantial and leads to the assumption that the polar studied inhibitor's adsorption at the carbon steel surface resulted in improved inhibitory efficiency.[68]

3.6. MD Simulation Study. A technique that can recreate the full inhibition system can be used to study theoretical insights on the inhibitor's ability to adsorb on steel surfaces. MD simulations are one of the most successful theoretical approaches to accomplish this.[69] With the aid of this technique, inhibitor metal interactions with a simulated solvent may be simulated, leading to outcomes that nearly resemble the actual adsorption process.[70] The Fe(110) plan, used in this study as a model of the carbon steel surface, was in contact with water molecules and one inhibitor molecule of TMAT or DMTMAT during MD simulations. As demonstrated in Figure 7, the triazole and thiophene moieties serve as a binding site for both inhibitors at Fe(110) with excess support for DMTMAT with the dimethylamine group. This result is in line with DFT analyses, and the experimental results that showed the DMTMAT molecule has a higher electron density than TMAT.

In this situation, it is anticipated that the molecules' reactive sites will interact physically and chemically, strengthening the carbon steel's resistance to dissolution.[71] Calculating the compound's interaction energy ($E_{interaction}$) using the Fe(110) plan is another method for figuring out the interacting force. To accomplish this, it is necessary to compute the single energies of the entire system (E_{total}), the inhibitor by itself ($E_{inhibitor}$), and the Fe(110) plan with the simulated solvent ($E_{surface+solution}$). The following equation links each of these variables:[72]

$$E_{interaction} = E_{total} - (E_{surface+solution} + E_{inhibitor}) \quad (13)$$

The interaction energies for TMAT and DMTMAT are −596 and −694 kJ/mol, respectively, based on obtained values. This implies that these molecules can firmly bind to the surface of carbon steel and provide increased surface coverage.[73] The radial distribution function (RDF), a crucial tool for determining the interatomic distance between the heteroatoms of the organic inhibitor and the metal surface, has been utilized to characterize the behavior of adsorption.[74] The literature substantiated that chemisorption is more advantageous when bond lengths are less than 3.5 Å. In contrast, physical adsorption is more expected if bond lengths are more than 3.5 Å.

Figure 8 displays that the bond-length values of TMAT and DMTMAT with the Fe atoms of the primary sheet are 2.46 and 2.41 Å, respectively. This shows that there is stronger defense because the TMAT and DMTMAT are firmly attached to the steel substrate. Furthermore, the bond length of Fe-

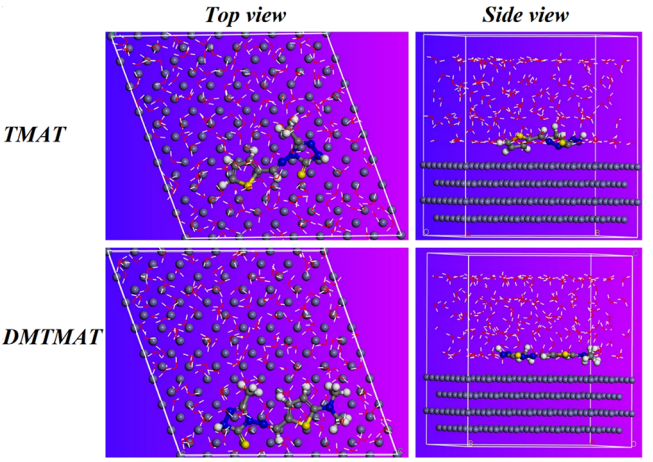

Figure 7. Top- and side-view simulations for TMAT and DMTMAT inhibitors at the Fe(110) surface.

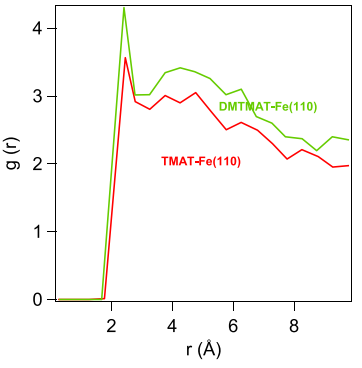

Figure 8. Radial distribution function (RDF) for TMAT and DMTMAT inhibitors at the Fe(110) surface.

https://doi.org/10.1021/acsomega.3c08127
ACS Omega 2024, 9, 6761−6772

Table 7. Inhibition Performance Comparison of Investigated Inhibitor with Other Schiff Bases

inhibitor	metal	electrolyte	inhibitor concentration	inhibition efficiency (%)	ref.
bis[5-(phenylazo)-2-hydroxybenzaldehyde]-4,4′-diaminophenylmethane	steel type XC70	HCl, 1 M DMSO	6×10^{-5} M	61.78	30
bis[5-(4-methylphenylazo)-2-hydroxybenzaldehyde]-4,4′-diaminophenylmethane				80.18	
bis[5-(4-bromophenylazo)-2-hydroxybenzaldehyde]-4,4′-diaminophenylmethane				52.72	
3-mercapto-2-((4-methoxybenzylidene)amino)propanoic acid	mild steel	1 M HCl	200 ppm	97.30	31
2-((4-hydroxy-3-methoxybenzylidene)amino)-3-mercaptopropanoic acid					
3-mercapto-2-(((*E*)-3-phenylallylidene)amino)propanoic acid					
3-((5-mercapto-1,3,4-thiadiazol-2-yl)imino)indolin-2-one	mild steel	1 M HCl	0.5 mM	96.90	32
2-hydroxy-*N*′-((thiophene-2-yl)methylene)benzohydrazide	mild steel	0.5 M H_2SO_4	4.06×10^{-4} M	98.11	79
o-hydroxy acetophenone benzoyl hydrazone	mild steel	1 M HCl	4.93×10^{-4} M	94.90	80
N′-(1-(2-hydroxyphenyl)ethylidene)acetohydrazide	mild steel	1 M HCl	300 mg L^{-1}	85.58	81
N′-(1-(2-hydroxyphenyl)ethylidene)benzohydrazide				85.73	
2-(1-(2-hydroxyphenyl)ethylidene)hydrazine-1-carbothioamide				86.52	
N′-(1-(2-hydroxyphenyl) ethylidene) hydrazinecarbothiohydrazide				92.41	
N (-benzo[d]thiazol-2-yl)-1-(thiophene-2-yl)methanimine	mild steel	1 M H_2SO_4	10.2×10^{-4} M	98.10	82
N,*N*′-(1,4-phenylenebis(methanylylidene))bis(5-(methylthio)-1,3,4-thiadiazol-2-amine	mild steel	1 M HCl	175 ppm	92.70	83
5,5′-((1,4-phenylenebis(methanylylidene))bis(azanylylidene))bis(1,3,4-thiadiazole-2-thiol)				91.10	
N,*N*′-(1,4-phenylenebis(methanylylidene))bis(5-methyl-1,3,4-thiadizol-2-amine)				87.8	
N,*N*′-(1,4-phenylenebis(methanylylidene))bis(1,3,4-thiadiazol-2-amine				80.50	
N-(benzo[*d*]thiazole-2-yl)-1-phenylethan-1-imines [*N*-(benzo[*d*]thiazole-2-yl)-1-phenylethan-1-imine			6 mg L^{-1}	79.00	84
N-(benzo[*d*]thiazole-2-yl)-1-(3-chlorophenyl) ethan-1-imine				85.00	
N-(benzo[*d*]thiazole-2-yl)-1-(*m*-tolyl) ethan-1-imine				88.00	
N-(benzo[*d*]thiazole-2-ylimino) ethyl) aniline				90.00	
the current TMAT	carbon steel		0.001 M	91.10	
the current DMTMAT				94.00	

https://doi.org/10.1021/acsomega.3c08127
ACS Omega 2024, 9, 6761−6772

DMTMAT has a lower bond length than Fe-TMAT, indicating improved adsorption and protection provided by DMTMAT.

3.7. Corrosion Inhibition Mechanism. Metal corrosion inhibition is mainly based on the adsorption of inhibitor molecules on the metal surface to form a protective layer. When inhibitor molecules combine with H^+ ions in an acidic environment, proton forms of the inhibitor are created.[75] This slows the corrosion process while also restricting the amount of H^+ ions that can interact with the metal. Additionally, inhibitor molecules prevent the metal surface from reducing oxygen, which results in oxygen reduction inhibition. Now, what is the nature of these adsorbed molecules? In fact, there are three possibilities: physisorption, chemisorption, or both. There is a number of evidence and observations that support the latter possibility. First, protonated inhibitor molecules can physically adsorb on the metal surface via electrostatic interaction with the oppositely charged electrolyte/metal interface. This can only happen if the metal surface or electrolyte/metal interface is negatively charged, so we now have to determine the surface charge. One can estimate this by calculating Fe-ZCP (zero charge potential) with the equation: $E_{corr} - E_q = 0$. A Fe-ZCP value >0 indicates that the surface is positively charged. Previous work reported that the eq value for steel in HCl is −530 mV vs SCE.[76] The maximum E_{corr} values were −527 and −528 mV vs SCE for TMAT and DMTMAT, respectively, as given in Table 4. Hence, the corresponding calculated Fe-ZCP values are +2 and +3 mV, respectively, indicating that the electrode surface is positively charged, while carbon steel in HCl solution is likely to be covered with negative chloride ions, resulting in an electrostatic interaction between negative chloride species and positively protonated inhibitor molecules at the electrolyte/metal interface, i.e., physisorption. The second is dependent on the chemical structure of the inhibitory molecules. They are likely to bind to the metal surface through donor−acceptor contacts resulting from the contact of the heteroatoms (N and/or S) of the triazole and thiophene rings of the inhibitors with the unoccupied d-orbital of the Fe atoms, i.e., chemisorption.[77,78] Third, the calculated thermodynamic aspects of the ΔG^{o}_{ads} values for TMAT and DMTMAT inhibitors were −36.7 and −38.5, as shown in Table 3, respectively, i.e., physisorption and chemisorption. Fourth, the bond-length values of heteroatoms in TMAT and DMTMAT with the Fe atoms of the primary sheet are less than 3.5 Å, as computed in theoretical investigations, which predicted the chemisorption mode of adsorption. Accordingly, the interaction of TMAT and DMTMAT inhibitors on the C-steel surface may occur through both physisorption and chemisorption, preventing corrosion. The anticorrosion efficiencies of a number of different Schiff bases are compared in Table 7.[30−32,79−84]

4. CONCLUSIONS

The performance of the synthesized triazole-thione Schiff bases (TMAT and DMTMAT) as corrosion inhibitors for carbon steel in 1 M HCl solution at a temperature of 298 K was evaluated using both experimental and computational methodologies. There was 91.1, 94.0, 90.3, 92.5, 90.5, and 92.5% agreement between the results of the gravimetric, PDP, and EIS investigations of the inhibitory efficacy of TMAT and DMTMAT, respectively. According to PDP measurements, the substances investigated behaved as mixed inhibitors. According to the EIS findings, the method of avoiding corrosion appeared to be the formation of a stable protective layer on the metal surface. For both inhibitors, a Langmuir isotherm was employed to fit the data. Adsorption can occur chemically or physically according to thermodynamic studies. The adsorption process is confirmed to be spontaneous by the negative values of the adsorption-free energy, which are −36.7 and −38.5 kJ/mol for TMAT and DMTMAT, respectively. Theoretical research findings from DFT and MD simulations are highly linked to experimental observations.

AUTHOR INFORMATION

Corresponding Authors

Arafat Toghan − *Chemistry Department, College of Science, Imam Mohammad Ibn Saud Islamic University (IMSIU), Riyadh 11623, Saudi Arabia; Chemistry Department, Faculty of Science, South Valley University, Qena 83523, Egypt*; orcid.org/0000-0002-1423-1147; Email: arafat.toghan@yahoo.com, aatahmed@imamu.edu.sa

Ahmed A. Farag − *Egyptian Petroleum Research Institute (EPRI), Cairo 11727, Egypt*; orcid.org/0000-0002-9019-5635; Email: ahmedafm@yahoo.com

Authors

Omar K. Alduaij − *Chemistry Department, College of Science, Imam Mohammad Ibn Saud Islamic University (IMSIU), Riyadh 11623, Saudi Arabia*

Ahmed Fawzy − *Chemistry Department, Faculty of Science, Assiut University, Assiut 71516, Egypt*

Ayman M. Mostafa − *Department of Physics, College of Science, Qassim University, Buraydah Almolaydah 51452, Saudi Arabia; Physics Research Institute, National Research Centre, Giza 12622, Egypt*

Ahmed M. Eldesoky − *Department of Chemistry, University College in Al-Qunfudhah, Umm Al-Qura University, Makkah 21912, Saudi Arabia*

Complete contact information is available at: https://pubs.acs.org/10.1021/acsomega.3c08127

Notes

The authors declare no competing financial interest.

ACKNOWLEDGMENTS

The authors extend their appreciation to the Deanship of Scientific Research at Imam Mohammad Ibn Saud Islamic University (IMSIU) for funding and supporting this work through Research Partnership Program no.RP-21-09-74.

REFERENCES

(1) Li, H.; Qiang, Y.; Zhao, W.; Zhang, S. A green Brassica oleracea L extract as a novel corrosion inhibitor for Q235 steel in two typical acid media. *Colloids Surfaces A Physicochem Eng. Asp.* **2021**, *616*, No. 126077.

(2) Esmaeili, N.; Neshati, J.; Yavari, I. Corrosion inhibition of new thiocarbohydrazides on the carbon steel in hydrochloric acid solution. *J. Ind. Eng. Chem.* **2015**, *22*, 159−163.

(3) Farag, A. A.; Eid, A. M.; Shaban, M. M.; Mohamed, E. A.; Raju, G. Integrated modeling, surface, electrochemical, and biocidal investigations of novel benzothiazoles as corrosion inhibitors for shale formation well stimulation. *J. Mol. Liq.* **2021**, *336*, No. 116315.

(4) Farag, A. A.; Badr, E. A. Non-ionic surfactant loaded on gel capsules to protect downhole tubes from produced water in acidizing oil wells. *Corros Rev.* **2020**, *38* (2), 151−164.

https://doi.org/10.1021/acsomega.3c08127
ACS Omega 2024, 9, 6761−6772

(5) Bijapur, K.; Molahalli, V.; Shetty, A.; Toghan, A.; De Padova, P.; Hegde, G. Recent Trends and Progress in Corrosion Inhibitors and Electrochemical Evaluation. *Appl. Sci.* **2023**, *13* (18), 10107.
(6) Olivares-Xometl, O.; López-Aguilar, C.; Herrastí-González, P.; et al. Adsorption and corrosion inhibition performance by three new ionic liquids on API 5L X52 steel surface in acid media. *Ind. Eng. Chem. Res.* **2014**, *53* (23), 9534−9543.
(7) Toghan, A.; Gadow, H. S.; Dardeer, H. M.; Elabbasy, H. M. New promising halogenated cyclic imides derivatives as potential corrosion inhibitors for carbon steel in hydrochloric acid solution. *J. Mol. Liq.* **2021**, *325*, No. 115136.
(8) Costa, E. M.; Dedavid, B. A.; Santos, C. A.; et al. Crevice corrosion on stainless steels in oil and gas industry: A review of techniques for evaluation, critical environmental factors and dissolved oxygen. *Eng. Fail Anal.* **2023**, *144*, No. 106955.
(9) Toghan, A.; Gadow, H. S.; Fawzy, A.; Alhussain, H.; Salah, H. Adsorption Mechanism, Kinetics, Thermodynamics, and Anticorrosion Performance of a New Thiophene Derivative for C-Steel in a 1.0 M HCl. *Experimental and Computational Approaches. Metals (Basel).* **2023**, *13* (9), 1565.
(10) Saleh, T. A.; Haruna, K.; Alharbi, B. Diaminoalkanes functionalized graphene oxide as corrosion inhibitors against carbon steel corrosion in simulated oil/gas well acidizing environment. *J. Colloid Interface Sci.* **2023**, *630*, 591−610.
(11) Odewunmi, N. A.; Mazumder, M. A. J.; Ali, S. A. Tipping effect of tetra-alkylammonium on the potency of N-(6-(1H-benzo[d]-imidazol-1-yl)hexyl)-N, N-dimethyldodecan-1-aminium bromide (BIDAB) as corrosion inhibitor of austenitic 304L stainless steel in oil and gas acidization: Experimental and DFT approac. *J. Mol. Liq.* **2022**, *360*, No. 119431.
(12) Toghan, A.; Fawzy, A. Unraveling the Adsorption Mechanism and Anti-Corrosion Functionality of Dextrin and Inulin as Eco-Friendly Biopolymers for the Corrosion of Reinforced Steel in 1.0 M HCl: A Thermodynamic and Kinetic Approach. *Polymers (Basel).* **2023**, *15* (14), 3144.
(13) Zhang, Q. H.; Li, Y. Y.; Lei, Y.; Wang, X.; Liu, H. F.; Zhang, G. A. Comparison of the synergistic inhibition mechanism of two eco-friendly amino acids combined corrosion inhibitors for carbon steel pipelines in oil and gas production. *Appl. Surf. Sci.* **2022**, *583*, No. 152559.
(14) Li, E.; Li, Y.; Liu, S.; Yao, P. Choline amino acid ionic liquids as green corrosion inhibitors of mild steel in acidic medium. *Colloids Surfaces A Physicochem Eng. Asp.* **2023**, *657*, No. 130541.
(15) Ouakki, M.; Galai, M.; Benzekri, Z.; et al. A detailed investigation on the corrosion inhibition effect of by newly synthesized pyran derivative on mild steel in 1.0 M HCl: Experimental, surface morphological (SEM-EDS, DRX& AFM) and computational analysis (DFT & MD simulation). *J. Mol. Liq.* **2021**, *344*, No. 117777.
(16) Al-Sabagh, A. M.; Abdou, M. I.; Migahed, M. A.; et al. Influence of ilmenite ore particles as pigment on the anticorrosion and mechanical performance properties of polyamine cured epoxy for internal coating of gas transmission pipelines. *Egypt J. Pet. Published online* **2018**, *27*, 427.
(17) Raviprabha, K.; Bhat, R. S. Inhibition Effects of Ethyl-2-Amino-4-Methyl-1,3-Thiazole-5-Carboxylate on the Corrosion of AA6061 Alloy in Hydrochloric Acid Media. *J. Fail Anal Prev.* **2019**, *19* (5), 1464−1474.
(18) Raviprabha, K.; Ramesh, S. Bhat 5-(3-Pryridyl)-4H-1,2,4-triazole-3-thiol as Potential Corrosion Inhibitor for AA6061 Aluminium Alloy in 0.1 M Hydrochloric Acid Solution. *Surf. Eng. Appl. Electrochem.* **2019**, *55* (6), 723−733.
(19) Raviprabha, K.; Bhat, R. S. Electrochemical and Quantum Chemical Studies of 5-[(4-Chlorophenoxy) Methyl]-4H-1,2,4-Triazole-3-Thiol on the Corrosion Inhibition of 6061 Al Alloy in Hydrochloric Acid. *J. Fail Anal Prev.* **2020**, *20* (5), 1598−1608.
(20) Raviprabha, K.; Bath, R. S. Corrosion Inhibition Effect of Ethyl 1-(4-chlorophenyl)-5-methyl-1H-1,2,3-triazole-4-carboxylate on Aluminium Alloy in Hydrochloric Acid. *Prot. Met. Phys. Chem. Surf.* **2021**, *57* (1), 181−189.
(21) Raviprabha, K.; Bhat, R. S. Corrosion inhibition of mild steel in 0.5 M HCL by substituted 1,3,4-oxadiazole. *Egypt J. Pet.* **2023**, *32* (2), 1−10.
(22) Al-Gamal, A. G.; Farag, A. A.; Elnaggar, E. M.; Kabel, K. I. Comparative impact of doping nano-conducting polymer with carbon and carbon oxide composites in alkyd binder as anti-corrosive coatings. *Compos Interfaces.* **2018**, *25* (11), 959−980.
(23) Haruna, K.; Obot, I. B.; Ankah, N. K.; Sorour, A. A.; Saleh, T. A. Gelatin: A green corrosion inhibitor for carbon steel in oil well acidizing environment. *J. Mol. Liq.* **2018**, *264*, 515−525.
(24) Farag, A. A.; Toghan, A.; Mostafa, M. S.; Lan, C.; Ge, G. Environmental Remediation through Catalytic Inhibition of Steel Corrosion by Schiff's Bases: Electrochemical and Biological Aspects. *Catalysts.* **2022**, *12* (8), 838.
(25) Migahed, M. A., Farag, A. A., Elsaed, S. M., Kamal, R., Abd El-Bary, H. Corrosion inhibition of carbon steel in formation water of oil wells by some schiff base non ionic surfactants. In: *European Corrosion Congress 2009*, EUROCORR 2009.; 2009. http://www.scopus.com/inward/record.url?eid=2-s2.0-77953707807&partnerID=MN8TOARS.
(26) Farag, A. A. Oil-in-water emulsion of a heterocyclic adduct as a novel inhibitor of API X52 steel corrosion in acidic solution. *Corros Rev.* **2018**, *36* (6), 575−588.
(27) Farag, A. A.; Mohamed, E. A.; Toghan, A. The new trends in corrosion control using superhydrophobic surfaces: a review. *Corros Rev.* **2023**, *41* (1), 21−37.
(28) Tourabi, M.; Nohair, K.; Traisnel, M.; Jama, C.; Bentiss, F. Electrochemical and XPS studies of the corrosion inhibition of carbon steel in hydrochloric acid pickling solutions. *Corros. Sci.* **2013**, *75*, 123−133.
(29) Mohamed, H. A.; Farag, A. A.; Badran, B. M. Corrosion inhibitiob of mild steel using emulsified thiazole adduct in Different binder systems. *Eurasian Chem. Technol. J.* **2008**, *10* (1), 67−77.
(30) Zobeidi, A.; Neghmouche Nacer, S.; Atia, S.; et al. Corrosion Inhibition of Azo Compounds Derived from Schiff Bases on Mild Steel (XC70) in (HCl, 1 M DMSO) Medium: An Experimental and Theoretical Study. *ACS Omega.* **2023**, *8* (24), 21571−21584.
(31) Gupta, N. K.; Quraishi, M. A.; Verma, C.; Mukherjee, A. K. Green Schiff's bases as corrosion inhibitors for mild steel in 1 M HCl solution: experimental and theoretical approach. *RSC Adv.* **2016**, *6* (104), 102076−102087.
(32) Betti, N.; Al-Amiery, A. A.; Al-Azzawi, W. K.; Isahak, WNRW Corrosion inhibition properties of schiff base derivative against mild steel in HCl environment complemented with DFT investigations. *Sci. Rep.* **2023**, *13* (1), 8979.
(33) Hu, C.; Li, T.; Yin, H.; Hu, L.; Tang, J.; Ren, K. Preparation and corrosion protection of three different acids doped polyaniline/epoxy resin composite coatings on carbon steel. *Colloids Surfaces A Physicochem Eng. Asp.* **2021**, *612*, No. 126069.
(34) Toghan, A.; Fawzy, A.; Alakhras, A. I.; Farag, A. A. Electrochemical and Theoretical Examination of Some Imine Compounds as Corrosion Inhibitors for Carbon Steel in Oil Wells Formation Water. *Int. J. Electrochem Sci.* **2022**, *17*, 2212108.
(35) Toghan, A.; Fawzy, A.; Alakhras, A. I.; et al. Experimental Exploration, RSM Modeling, and DFT/MD Simulations of the Anticorrosion Performance of Naturally Occurring Amygdalin and Raffinose for Aluminum in NaOH Solution. *Coatings.* **2023**, *13* (4), 704.
(36) Mohamed, E. A.; Altalhi, A. A.; Amer, A.; Negm, N. A.; Azmy, E. A. M.; Farag, A. A. Two novel Schiff bases derived from 3-amino-1,2,4-triazole as corrosion inhibitors for carbon steel pipelines during acidizing treatment of oil wells: Laboratory and theoretical studies. *Energy Sources, Part A Recover Util Environ. Eff.* **2023**, *45* (2), 3246−3265.
(37) Farag, A. A.; Abdallah, H. E.; Badr, E. A.; Mohamed, E. A.; Ali, A. I.; El-Etre, A. Y. The inhibition performance of morpholinium derivatives on corrosion behavior of carbon steel in the acidized

https://doi.org/10.1021/acsomega.3c08127
ACS Omega 2024, 9, 6761−6772

formation water: Theoretical, experimental and biocidal evaluations. *J. Mol. Liq.* **2021**, *341*, No. 117348.
(38) Dehghani, A.; Bahlakeh, G.; Ramezanzadeh, B.; Ramezanzadeh, M. Potential of Borage flower aqueous extract as an environmentally sustainable corrosion inhibitor for acid corrosion of mild steel: Electrochemical and theoretical studies. *J. Mol. Liq.* **2019**, *277*, 895−911.
(39) Boricha, A. G.; Murthy, Z. V. P. Preparation of N,O-carboxymethyl chitosan/cellulose acetate blend nanofiltration membrane and testing its performance in treating industrial wastewater. *Chem. Eng. J.* **2010**, *157* (2), 393−400.
(40) Shi, H.; Dong, C.; Yang, Y.; et al. Preparation of sulfonate chitosan microspheres and study on its adsorption properties for methylene blue. *Int. J. Biol. Macromol.* **2020**, *163*, 2334−2345.
(41) Shaban, S. M.; Badr, E a; Shenashen, M. A.; Farag, A. A. Fabrication and characterization of encapsulated Gemini cationic surfactant as anticorrosion material for carbon steel protection in down-hole pipelines. *Environ. Technol. Innov.* **2021**, *23*, No. 101603.
(42) Fawzy, A.; Toghan, A.; Alqarni, N.; et al. Experimental and Computational Exploration of Chitin, Pectin, and Amylopectin Polymers as Efficient Eco-Friendly Corrosion Inhibitors for Mild Steel in an Acidic Environment. Kinetic, Thermodynamic, and Mechanistic Aspects. *Polymers (Basel).* **2023**, *15* (4), 891.
(43) Hu, K.; Zhuang, J.; Ding, J.; Ma, Z.; Wang, F.; Zeng, X. Influence of biomacromolecule DNA corrosion inhibitor on carbon steel. *Corros. Sci.* **2017**, *125*, 68−76.
(44) Chen, L.; Hao, H. Y.; Zhang, W. T.; Shao, Z. Adsorption mechanism of copper ions in aqueous solution by chitosan−carboxymethyl starch composites. *J. Appl. Polym. Sci.* **2020**, *137* (18), 1−10.
(45) Vengatesh, G.; Sundaravadivelu, M. Non-toxic bisacodyl as an effective corrosion inhibitor for mild steel in 1 M HCl: Thermodynamic, electrochemical, SEM, EDX, AFM, FT-IR, DFT and molecular dynamics simulation studies. *J. Mol. Liq.* **2019**, *287*, No. 110906.
(46) Likhanova, N. V.; Arellanes-Lozada, P.; Olivares-Xometl, O.; et al. Effect of organic anions on ionic liquids as corrosion inhibitors of steel in sulfuric acid solution. *J. Mol. Liq.* **2019**, *279*, 267−278.
(47) Shan, C. X.; Hou, X.; Choy, K. L. Corrosion resistance of TiO2 films grown on stainless steel by atomic layer deposition. *Surf. Coat. Technol.* **2008**, *202* (11), 2399−2402.
(48) Assad, H.; Kumar, A. Understanding functional group effect on corrosion inhibition efficiency of selected organic compounds. *J. Mol. Liq.* **2021**, *344*, No. 117755.
(49) Dehghani, A.; Ramezanzadeh, B. Rosemary extract inhibitive behavior against mild steel corrosion in tempered 1 M HCl media. *Ind. Crops Prod.* **2023**, *193*, No. 116183.
(50) Moretti, G.; Guidi, F.; Fabris, F. Corrosion inhibition of the mild steel in 0.5M HCl by 2-butyl-hexahydropyrrolo[1,2-b][1,2]-oxazole. *Corros. Sci.* **2013**, *76*, 206−218.
(51) Aljourani, J.; Raeissi, K.; Golozar, M. A. Benzimidazole and its derivatives as corrosion inhibitors for mild steel in 1M HCl solution. *Corros. Sci.* **2009**, *51* (8), 1836−1843.
(52) Dehri, İ; Özcan, M. The effect of temperature on the corrosion of mild steel in acidic media in the presence of some sulphur-containing organic compounds. *Mater. Chem. Phys.* **2006**, *98* (2), 316−323.
(53) Toghan, A.; Fawzy, A.; Alakhras, A. I.; Sanad, M. M. S.; Khairy, M.; Farag, A. A. Correlating Experimental with Theoretical Studies for a New Ionic Liquid for Inhibiting Corrosion of Carbon Steel during Oil Well Acidification. *Metals (Basel).* **2023**, *13* (5), 862.
(54) Mashuga, M. E.; Olasunkanmi, L. O.; Lgaz, H.; Sherif, E. S. M.; Ebenso, E. E. Aminomethylpyridazine isomers as corrosion inhibitors for mild steel in 1 M HCl: Electrochemical, DFT and Monte Carlo simulation studies. *J. Mol. Liq.* **2021**, *344*, No. 117882.
(55) Toghan, A.; Khairy, M.; Huang, M.; Farag, A. A. Electrochemical, chemical and theoretical exploration of the corrosion inhibition of carbon steel with new imidazole-carboxamide derivatives in an acidic environment. *Int. J. Electrochem Sci.* **2023**, *18* (3), No. 100072.
(56) Olasunkanmi, L. O.; Aniki, N. I.; Adekunle, A. S.; et al. Investigating the synergism of some hydrazinecarboxamides and iodide ions as corrosion inhibitor formulations for mild steel in hydrochloric Acid: Experimental and computational studies. *J. Mol. Liq.* **2021**, *343*, No. 117600.
(57) El Bakri, Y.; Guo, L.; Anouar, E. H.; Essassi, E. M. Electrochemical, DFT and MD simulation of newly synthesized triazolotriazepine derivatives as corrosion inhibitors for carbon steel in 1 M HCl. *J. Mol. Liq.* **2019**, *274*, 759−769.
(58) Dueke-Eze, C. U.; Madueke, N. A.; Iroha, N. B.; et al. Adsorption and inhibition study of N-(5-methoxy-2-hydroxybenzylidene) isonicotinohydrazide Schiff base on copper corrosion in 3.5% NaCl. *Egypt J. Pet.* **2022**, *31* (2), 31−37.
(59) Jeeva, M.; Boobalan, M. S.; Prabhu, G. V. Adsorption and anticorrosion behavior of 1-((pyridin-2-ylamino)(pyridin-4-yl)-methyl)pyrrolidine-2,5-dione on mild steel surface in hydrochloric acid solution. *Res. Chem. Intermed.* **2018**, *44* (1), 425−454.
(60) Toghan, A.; Fawzy, A.; Al Bahir, A.; et al. Computational Foretelling and Experimental Implementation of the Performance of Polyacrylic Acid and Polyacrylamide Polymers as Eco-Friendly Corrosion Inhibitors for Copper in Nitric Acid. *Polymers (Basel).* **2022**, *14* (22), 4802.
(61) Haque, J.; Ansari, K. R.; Srivastava, V.; Quraishi, M. A.; Obot, I. B. Pyrimidine derivatives as novel acidizing corrosion inhibitors for N80 steel useful for petroleum industry: A combined experimental and theoretical approach. *J. Ind. Eng. Chem.* **2017**, *49*, 176−188.
(62) Elemike, E. E.; Onwudiwe, D. C.; Nwankwo, H. U.; Hosten, E. C. Synthesis, crystal structure, electrochemical and anti-corrosion studies of Schiff base derived from o-toluidine and o-chlorobenzaldehyde. *J. Mol. Struct.* **2017**, *1136*, 253−262.
(63) Sengupta, S.; Murmu, M.; Mandal, S.; Hirani, H.; Banerjee, P. Competitive corrosion inhibition performance of alkyl/acyl substituted 2-(2-hydroxybenzylideneamino)phenol protecting mild steel used in adverse acidic medium: A dual approach analysis using FMOs/molecular dynamics simulation corroborated experimental fin. *Colloids Surfaces A Physicochem Eng. Asp.* **2021**, *617*, No. 126314.
(64) Odewunmi, N. A.; Mazumder, M. A. J.; Ali, S. A. Tipping effect of tetra-alkylammonium on the potency of N-(6-(1H-benzo[d]-imidazol-1-yl)hexyl)-N, N-dimethyldodecan-1-aminium bromide (BIDAB) as corrosion inhibitor of austenitic 304L stainless steel in oil and gas acidization: Experimental and DFT approach. *J. Mol. Liq.* **2022**, *360*, No. 119431.
(65) Momeni, M. J.; Behzadi, H.; Roonasi, P.; Sadjadi, S. A. S.; Mousavi-Khoshdel, S. M.; Mousavi, S. V. Ab initio study of two quinoline derivatives as corrosion inhibitor in acidic media: electronic structure, inhibitor−metal interaction, and nuclear quadrupole resonance parameters. *Res. Chem. Intermed.* **2015**, *41* (9), 6789−6802.
(66) El Hassani, A. A.; El Adnani, Z.; Benjelloun, A. T.; et al. DFT Theoretical Study of 5-(4-R-Phenyl)-1H-tetrazole (R = H; OCH3; CH3; Cl) as Corrosion Inhibitors for Mild Steel in Hydrochloric Acid. *Met Mater. Int.* **2020**, *26* (11), 1725−1733.
(67) Shahraki, M.; Dehdab, M.; Elmi, S. Theoretical studies on the corrosion inhibition performance of three amine derivatives on carbon steel: Molecular dynamics simulation and density functional theory approaches. *J. Taiwan Inst Chem. Eng.* **2016**, *62*, 313−321.
(68) Gece, G.; Bilgiç, S. Quantum chemical study of some cyclic nitrogen compounds as corrosion inhibitors of steel in NaCl media. *Corros. Sci.* **2009**, *51* (8), 1876−1878.
(69) Abdelaziz, S.; Benamira, M.; Messaadia, L.; Boughoues, Y.; Lahmar, H.; Boudjerda, A. Green corrosion inhibition of mild steel in HCl medium using leaves extract of Arbutus unedo L. plant: An experimental and computational approach. *Colloids Surfaces A Physicochem Eng. Asp.* **2021**, *619*, No. 126496.
(70) Mohamed, E. A.; Hashem, H. E.; Azmy, E. M.; Negm, N. A.; Farag, A. A. Synthesis, structural analysis, and inhibition approach of novel eco-friendly chalcone derivatives on API X65 steel corrosion in

https://doi.org/10.1021/acsomega.3c08127
ACS Omega 2024, 9, 6761−6772

acidic media assessment with DFT & MD studies. *Environ. Technol. Innovation* **2021**, *24*, No. 101966.
(71) Farag, A. A.; Ismail, A. S.; Migahed, M. A. Squid By-product Gelatin Polymer as an Eco-friendly Corrosion Inhibitor for Carbon Steel in 0.5 M H2SO4 Solution: Experimental, Theoretical, and Monte Carlo Simulation Studies. *J. Bio- Tribo-Corros.* **2020**, *6* (1), 16 DOI: 10.1007/s40735-019-0310-0.
(72) Hashem, H. E.; Farag, A. A.; Mohamed, E. A.; Azmy, E. M. Experimental and theoretical assessment of benzopyran compounds as inhibitors to steel corrosion in aggressive acid solution. *J. Mol. Struct.* **2022**, *1249*, No. 131641.
(73) Qiang, Y.; Zhang, S.; Guo, L.; Zheng, X.; Xiang, B.; Chen, S. Experimental and theoretical studies of four allyl imidazolium-based ionic liquids as green inhibitors for copper corrosion in sulfuric acid. *Corros. Sci.* **2017**, *119*, 68−78.
(74) Mehmeti, V.; Podvorica, F. I. Experimental and Theoretical Studies on Corrosion Inhibition of Niobium and Tantalum Surfaces by Carboxylated Graphene Oxide. *Materials (Basel).* **2018**, *11* (6), 893.
(75) Mobin, M.; Aslam, R.; Salim, R.; Kaya, S. An investigation on the synthesis, characterization and anti-corrosion properties of choline based ionic liquids as novel and environmentally friendly inhibitors for mild steel corrosion in 5% HCl. *J. Colloid Interface Sci.* **2022**, *620*, 293−312.
(76) Chen, G.; Zhang, M.; Zhao, J.; Zhou, R.; Meng, Z.; Zhang, J. Investigation of ginkgo biloba leave extracts as corrosion and Oil field microorganism inhibitors. *Chem. Cent J.* **2013**, *7* (1), 83.
(77) Shaban, M. M.; Negm, N. A.; Farag, R. K.; et al. Anti-corrosion, antiscalant and anti-microbial performance of some synthesized trimeric cationic imidazolium salts in oilfield applications. *J. Mol. Liq.* **2022**, *351*, No. 118610.
(78) Saranya, J.; Sowmiya, M.; Sounthari, P.; Parameswari, K.; Chitra, S.; Senthilkumar, K. N-heterocycles as corrosion inhibitors for mild steel in acid medium. *J. Mol. Liq.* **2016**, *216*, 42−52.
(79) Singh, A. K.; Thakur, S.; Pani, B.; Ebenso, E. E.; Quraishi, M. A.; Pandey, A. K. 2-Hydroxy- N ′-((Thiophene-2-yl)methylene)-benzohydrazide: Ultrasound-Assisted Synthesis and Corrosion Inhibition Study. *ACS Omega.* **2018**, *3* (4), 4695−4705.
(80) Singh, A. K.; Singh, P. Adsorption behaviour of o-hydroxy acetophenone benzoyl hydrazone on mild steel/hydrochloric acid interface. *J. Ind. Eng. Chem.* **2015**, *21*, 552−560.
(81) Singh, A. K.; Chugh, B.; Singh, M.; et al. Hydroxy phenyl hydrazides and their role as corrosion impeding agent: A detail experimental and theoretical study. *J. Mol. Liq.* **2021**, *330*, No. 115605.
(82) Singh, A. K.; Singh, M.; Thakur, S.; et al. Adsorption study of N (-benzo[d]thiazol-2-yl)-1-(thiophene-2-yl) methanimine at mild steel/aqueous H2SO4 interface. *Surfaces and Interfaces.* **2022**, *33*, No. 102169.
(83) Chugh, B.; Singh, A. K.; Thakur, S.; et al. Comparative Investigation of Corrosion-Mitigating Behavior of Thiadiazole-Derived Bis-Schiff Bases for Mild Steel in Acid Medium: Experimental, Theoretical, and Surface Study. *ACS Omega.* **2020**, *5* (23), 13503−13520.
(84) Chugh, B.; Singh, A. K.; Thakur, S.; et al. An Exploration about the Interaction of Mild Steel with Hydrochloric Acid in the Presence of N -(Benzo[d]thiazole-2-yl)-1-phenylethan-1-imines. *J. Phys. Chem. C* **2019**, *123* (37), 22897−22917.

https://doi.org/10.1021/acsomega.3c08127
ACS Omega 2024, 9, 6761−6772